Membrane Water Treatment, Vol. 2, No. 4 (2011) 251-266
DOI: http://dx.doi.org/10.12989/mwt.2011.2.4.251

The use of HRSEM to characterize new and aged membranes in drinking water production

Y. Wyart[1], S. Nitsche[2], D. Chaudanson[2], K. Glucina[3] and P. Moulin[1]*

[1]*Laboratoire de Mécanique, Modélisation et Procédés Propres (M2P2-CNRS-UMR 6181), Université Paul Cézanne Aix Marseille, Europôle de l'Arbois, BP 80, Bat. Laennec, Hall C, 13545 Aix en Provence cedex 04, France*
[2]*Centre Interdisciplinaire de Nanoscience de Marseille (CINaM-UPR 3138), Campus de Luminy, 13288 Marseille Cedex 09, France*
[3]*SUEZ ENVIRONNEMENT, CIRSEE, Pôle Qualité Eau, 38, rue du Président-Wilson, 78230 Le Pecq, France*

(Received October 14, 2010, Revised September 12, 2011, Accepted October 5, 2011)

Abstract. This work deals with the use of High Resolution Scanning Electron Microscopy (HRSEM) to verify ultrafiltration membrane selectivity at the end of the production line as well as membrane ageing. The first part of this work is focused on new membranes. It is shown that it is better to use sputtering metallization than vacuum deposition, as this latter technique entails thermal damage to the skin layer. Moreover, the impact of the metallization layer on the determination of the membrane pore size is studied and it is observed that no impact of the metallization step can be clearly defined for a metallization layer ranging from 3 to 12 nm. For example, an average pore size of 16.9 nm and a recovery rate of 6.5 % are observed for a 150 kDa cellulose acetate membrane. These results are in agreement with those given by the manufacturer: pore size ranging from 10 to 15 nm and recovery rate ranging from 5 to 10 %. The second part of this work focuses on the study of membrane ageing. A PVDF hollow fibre membrane is studied. It is shown that a 65 % decrease in the permeate flux can be linked to a decrease in the number of pores at the surface of the membrane and a decrease in the recovery rate. In conclusion, a mapping of the pores is performed for several new hollow fibre membranes used to produce drinking water, made of different materials, with different geometries and molecular weight cut-off. These results provide reference data that will help better understand the phenomena of membrane fouling and membrane ageing.

Keywords: HRSEM; mapping; drinking water; membrane ageing

I. Introduction

The use of membrane technology for water treatment is growing steadily by 20% every year. Indeed, ultrafiltration and nanofiltration / reverse osmosis are increasingly used to produce drinking water from fresh water and salt water, respectively. However a major drawback in the development of membrane processes is membrane fouling. During the filtration step, fouling can occur either on the membrane surface or within the pores. This phenomenon can lead to a reduction in the production in terms of permeate flux and/or selectivity. A great number of studies have been carried out to gain a better understanding of membrane fouling and so limit its effects (Chan and Chan 2004, Chen *et al*. 2004, Pontie *et al*. 2005). In this way, membrane structure parameters (porosity, roughness,

* Corresponding author, Professor, E-mail: philippe.moulin@univ-cezanne.fr

pore size, pore shape and pore size distribution) and membrane/effluent coupling parameters (membrane material, surface charge, hydrophobicity, etc) can be taken into account. Advances in the study of membrane structure have been made thanks to microscopic techniques such as Scanning Electron Microscopy (SEM) (Wu and Wu 1995), Transmission Electron Microscopy (TEM) (Sheldon 1991), Atomic Force Microscopy (AFM) (Bottino *et al*. 1994) and Scanning Tunnelling Microscopy (STM) (Chahboun *et al*. 1992). Among these various techniques, the most widely used is SEM even though this technique entails a less accurate pore size determination (Kim *et al*. 1999). SEM is especially used for the characterization of the structure of MF (low pressure ultrafiltration) and UF (ultrafiltration) membranes (Xiuli *et al*. 1998) and for the study of the fouling phenomenon.

At the beginning of the 90s, SEM was increasingly used to obtain a good visualization of the membrane structure. Zeman and Denault (1992) used SEM associated with a computerized quantitative image analysis to characterize cellulose MF membranes. They focused on the impact of several factors such as image contrast, resolution and grey-level segmenting threshold on image treatment and analysis. Kim *et al*. (1990) were the first to use Field Emission Scanning Electron Microscopy (FESEM) to obtain micrographs of the top skin layer of various ultrafiltration membranes at low accelerating voltage (2-5 kV). Low surface porosities (< 10 %) and wide pore size distributions were observed. FESEM, also called HRSEM, was developed to observe under an electron beam fragile materials such as polymers (Tagawa *et al*. 1978), semiconductors (Meieran and Kamins 1973) and biological cells (Alen and Goldberg 1993). SEM and HRSEM differ mainly in their most important part: the electron gun, whose function is to provide a large and stable current in a small beam. SEM is equipped with a thermionic emission electron gun whereas HRSEM is generally equipped with a field emission electron gun. As the theoretical brightness of the field emission electron gun is 100 times higher than that of the thermionic emission electron gun, HRSEM is used to obtain a stronger detection signal when the spot on the sample is very small. Compared to SEM, HRSEM produces a cleaner image, fewer electrostatic distortions, and reaches a spatial resolution < 2nm. More information on the differences between SEM and HRSEM was given by Kim and Fane (1994).

SEM can give the pore size distribution of the membrane skin layer. From a cross-section view, it is also possible to obtain information about the membrane bulk, such as the number of layers that constitute the ceramic membrane (Wyart *et al*. 2008). To obtain more information about the membrane bulk, it is necessary to use SEM combined with other techniques. Hernandez *et al*. (1998) characterized Clyclopore and Nuclepore membranes with a nominal pore diameter ranging from 0.1 to 1 μm and from 0.015 to 5 μm, respectively. Bulk characteristics were obtained using a mercury intrusion apparatus, an extended bubble point method and a gas adsorption–desorption technique while surface characterization was carried out using Atomic Force Spectroscopy (AFM) and SEM. In that study, a link was made between water permeability and the pore size obtained using each technique and it was concluded that permeability is function of the bulk characteristics while selectivity and retention are function of surface characteristics. Ziel *et al*. (2008) combined SEM and TEM to obtain the porosity profiles of PES (polyethersulfone) membranes with 0.2 μm nominal pore size.

SEM results can also be linked with operating measurements such as the rejection rate. Masselin *et al*. (2001) studied 5 UF membranes made of different materials (PES, PVDF and PAN) using FESEM imaging and NIH (National Institutes of Health) image analysis software. They showed that the pore radiuses obtained from image analysis were in agreement with the rejection results. Wickramasinghe *et al*. (2009) worked on a very interesting topic and succeeded in linking the pore size distribution of UF membranes (100, 300 and 1000 kDa) obtained using Field-Emission Scanning Electron Microscopy with dextran rejection.

SEM - used alone or combined with AFM – is a very powerful technique to study the fouling phenomenon. Hwang and Lin (2002) used SEM to observe the fouling of MF membranes after filtration of calibrated particles (mean diameter = 0.4 μm). Fouling was standard for open and large surface pores, complete for uniform cylindrical pores and intermediate for interconnected and tortuous pores. Warczock *et al*. (2004) used SEM to obtain cross-section images of nanofiltration membranes in order to observe the thickness of the fouling layer and the blocking of the skin layer pores.

The combined use of SEM and AFM makes it possible to set up rules governing the choice of membranes. Hirose *et al*. (1996) synthesized 6 cross-linked aromatic polyamide membranes and showed that the roughest membranes provided the best performances in terms of flux - the flux increasing quasi-linearly with the membrane roughness. This was attributed to the fact that the increase in membrane roughness corresponds to an increase in effective filtration area. Elimelech *et al*. (1997) observed a higher permeate flux and a faster flux decline for a cellulose acetate membrane than for a polyamide composite membrane (which is rougher).

The purpose of this study is to show the limits and adequacy of the measurements obtained with high resolution SEM. In the field of membranes, this analytical technique is multipurpose since it makes it possible to characterize membranes throughout their life, from the very characterization at the end of the production line up to an expertise performed after a drop in production.

2. Material and methods

2.1 Membranes

Several membranes of different types and geometries were analyzed. Table 1 summarizes the main characteristics of these membranes and highlights the importance of treating these membranes. As ceramic membranes are not degraded by the electron beam, they are used as reference, while organic membranes are used to determine membrane structural parameters. For that purpose, a mapping of membranes A at the end of the production line and an ageing study of membranes B were performed.

A dynamic cleaning of membranes A was performed before each observation in order to remove glycerine and other conditioning products. This cleaning consisted in successive one-hour filtrations of acid (citric acid, pH = 4) and basic (soda pH = 8.5) solutions under low transmembrane pressure

Table 1 Summary of studied membranes

Membrane	Geometry	MWCO (kDa)	Material	Diameter	Interest
Ceramic	Tubular	150	-	-	(i) weak metallization (ii) no structure modification by electron beam (iii) determination of the metallization layer influence on the visualization
A	Hollow fiber Internal skin	100	Cellulose acetate	0.93-1.66	Membrane cartography at the end of the production step
B	Hollow fiber External skin	100	PVDF	0.47-0.7	Study of membrane ageing

(TMP = 0.1 bar). Rinsing was performed before the first filtration (acid solution), then before the second filtration (basic solution) and finally after the basic solution filtration, each time at the same TMP at the rate of 300 $L.m^{-2}$.

Two types of membrane B were characterized. AB (Aged B) membranes were membranes B extracted from the process after a backwash and CB (Clean B) membranes were AB membranes washed by chemical cleaning. This chemical cleaning was carried out in 2 steps: first an alkaline solution containing 500 ppm of Cl_2 was filtered for 5 hours to remove the organic fouling and then a solution of citric acid (pH = 2.2) was filtered for 5 hours to remove the mineral fouling.

2.2 Metal coaters

For the study of new and used membranes, three different metal coaters were tested:
- a JEOL gold sputter coater,
- an Edwards 306 evaporator for gold metallization - the metallization layer thickness being controlled with a quartz balance,
- a 4 magnetron sputtering apparatus for titanium metallization by sputtering – the metallization layer thickness depends on the previously calibrated exposition time.

2.3. Image processing software

In this study, the Leica QWin software, especially designed for quantitative microscopy, was used for image analysis and processing. With this software, it was possible to obtain information about the equivalent pore diameter and the recovery rate. As the pores detected are irregularly-shaped objects, the equivalent pore diameter, defined as the diameter of a disc of equivalent area, is used to compare different membranes. The recovery rate is defined as the ratio of pore area to membrane area.

3. Results

3.1 Effects of the metallization step on ceramic membranes

The impact of the conductive material layer deposited during metallization on the pore size determination was also studied here. For that purpose, a ceramic membrane with MWCO of 150 kDa, similar to those used for drinking water production, was taken as reference and various Ti thicknesses (0, 3, 6, 9 and 12 nm) were tested. Two observation windows - magnification × 40,000 and × 80,000 - were used. These two magnifications were chosen to work on objects in sufficient number so that representative statistical data on the entire membrane can be obtained. For magnifications lower than × 40,000, the objects to consider were very numerous and image processing was more random. For magnifications higher than × 80,000, the objects to consider were not in sufficient number and the results were not statistically satisfying. Initially it was observed that unfortunately the images cannot be exploited without prior metallization (Fig. 1).

Fig. 1 shows very dark overflowing areas. These areas did not allow continuous drainage of the charges of the membrane surface, resulting in an accumulation of charges. In this case, the SEM observations are of poor quality.

This section of the study focuses on the processing of 27 images: 14 images for a × 40,000

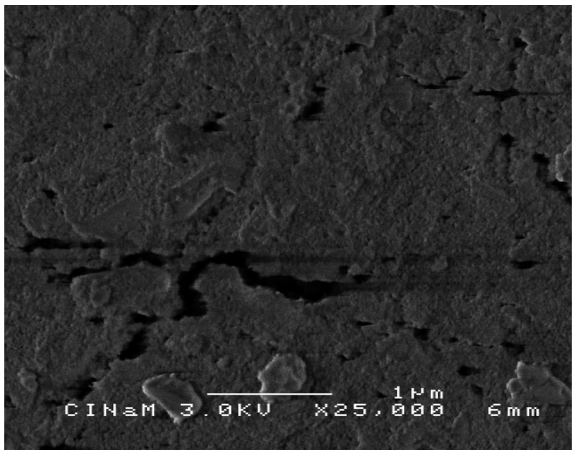

Fig. 1 Visualisation of a 150 kDa ceramic membrane without metallization step

Table 2 Results of image treatment and analysis for ceramic membrane with × 40,000 magnification

Metallization layer (nm)	Sample number	Pore number	Pore equivalent diameter (nm)		Recovery rate (%)	
			Average	Standard deviation	Average	Standard deviation
3	2	643	19.1	1.9	4.9	1.2
6	4	582	21.0	1.3	5.7	1.2
9	4	460	23.6	1.1	5.7	0.8
12	4	570	21.3	1.2	5.5	1.0
Average	-	564	21.3	-	5.5	-

Table 3 Results of image treatment and analysis for ceramic membrane with × 80,000 magnification

Metallization layer (nm)	Sample number	Pore number	Pore equivalent diameter (nm)		Recovery rate (%)	
			Average	Standard deviation	Average	Standard deviation
3	1	308	18.2	-	10.9	-
6	4	363	17.4	2.3	11.7	5.3
9	4	209	20.2	2.2	8.6	2.0
12	4	297	16.9	0.6	8.5	3.0
Average	-	294	18.2	-	9.9	-

magnification and 13 for a × 80,000 magnification. For each image, the information obtained concerns the mean equivalent pore diameter and the recovery rate. All the results are summarized in Table 2 for the × 40,000 magnification and in Table 3 for × 80,000 magnification.

In view of the results in Tables 2 and 3, it can be concluded that the metallization step has no influence on the determination of the equivalent pore diameter and of the recovery rate in a 3 to 12 nm thick metallization layer. For × 40,000 magnification (Table 2), an average equivalent pore diameter of 21.3 nm is obtained, with a minimum value of 19.1 nm (metallization layer thickness = 3 nm) and a maximum value of 23.6 nm (metallization layer thickness = 9 nm). The gap between the minimum and the maximum values is 4.5 nm, which corresponds to the smallest element of

definition (pixel) for a magnification of 40,000 (1 pixel = 4.44 nm). This confirms the fact that a metallization layer thickness ranging from 3 to 12 nm has no effect on the results. A similar observation can be made for the recovery rate. Finally, it is interesting to note that the minimum measurable diameter is set by our applications and it corresponds here to a square with a side length of 2 pixels. For × 80,000 magnification (Table 3), an average equivalent pore diameter of 18.2 nm is obtained, with a minimum value of 16.9 nm (metallization layer thickness = 12 nm) and a maximum value of 20.2 nm (metallization layer thickness = 9 nm). The gap between the minimum and maximum values is 3.3 nm, which is not significant since the size of the smallest element of definition (a pixel) is 2.22 nm for an × 80,000 magnification. This confirms the observation made for an × 40,000 magnification: a metallization layer thickness ranging from 3 to 12 nm does not affect the results, no matter the magnification. Finally, it is interesting to note that the minimum measurable diameter corresponds here to a square with a side length of 2 pixels.

Now, a reflection can be conducted on the influence of the observation scale on the results obtained. A first remark concerns the number of pores detected: there are twice as many pores for a × 40,000 magnification (564 on average) as for a × 80,000 magnification (294 on average), which seems perfectly logical. In order to determine the minimum diameter, a reference element of the same number of pixels (i.e., 2) was used. This may explain the fact that when one starts counting pores from 5.0 nm (× 80,000 magnification), the average equivalent pore diameter is smaller (18.2 nm) than when one counts pores from 8.7 nm (× 40,000 magnification, average equivalent pore diameter = 21.3 nm). However, this difference is not significant to within about 1 pixel with regard to the magnification. Then again, counting smaller pores for a × 80,000 magnification seems to have an influence on the determination of the recovery rate: it is twice as high for a × 80,000 magnification as for a × 40,000 magnification. On the other hand, for both cases, the results obtained are the same as those given by the membranes manufacturer: recovery rate between 5 and 10 %.

To conclude this section, it appears that a × 80,000 magnification is optimal because it makes it possible to work on a sufficient number of objects to be processed for quantitative statistical analysis, with an easier image processing step than for a × 40,000 magnification. It has already been demonstrated that such observations allow the determination of the cut-off of ceramic membranes (Wyart *et al*. 2008).

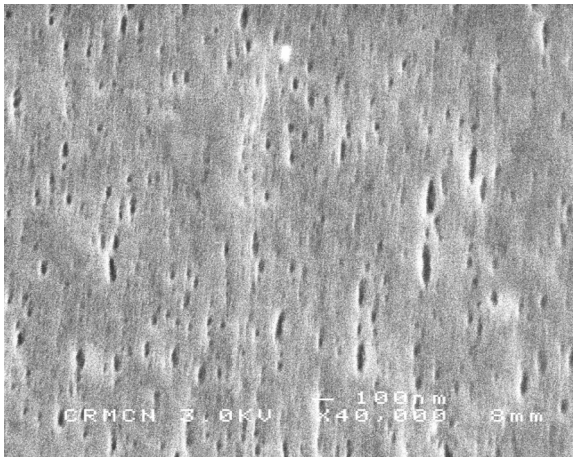

Fig. 2 Internal skin visualization of A membrane with a 5 nm gold layer (× 40,000 magnification)

3.2 Mapping of new membranes

3.2.1 Cellulose acetate membranes (membranes A)

Cellulose acetate membranes are very sensitive to heat and thermal deterioration occurs very rapidly if the electron beam remains close to the membrane for too long. Therefore, focusing must be done at a different spot from that of shooting, and this does not make it possible to get two images of the same spot. Fig. 2 shows the surface of the internal skin of the cellulose acetate membrane. It can be observed that the pores have an elongated shape in the direction of the vertical

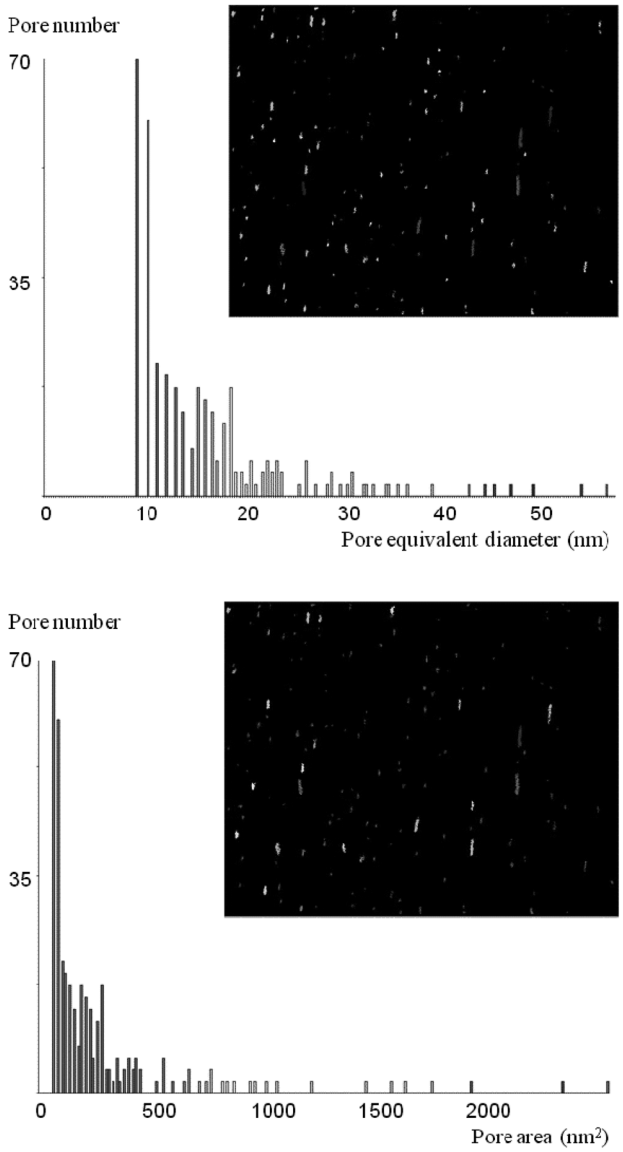

Fig. 3 Variation of pore number according to pore equivalent diameter (at the top) and pore area (at the bottom) for A membrane, × 40,000 magnification

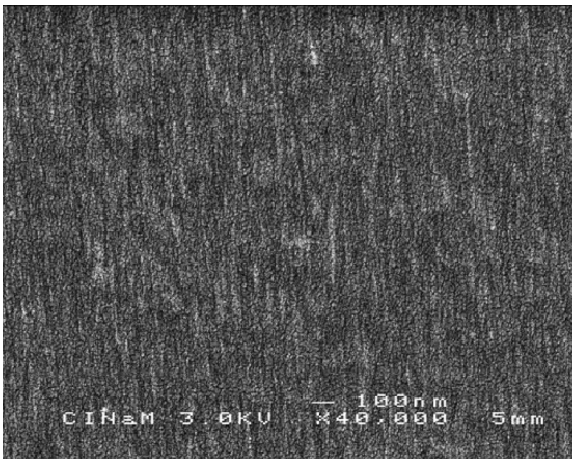

Fig. 4 Internal skin visualization of A membrane prepared by vapor deposition (× 40,000 magnification)

axis of the hollow fibers, that is to say, in the direction of the production nozzle.

Fig. 3 shows the image processing related to the fluctuations in pore number according to the pore diameter and the pore area. For 396 detected pores, the equivalent pore diameters range from 9.4 to 56.9 nm, with an average value of 16.9 nm. This value is consistent with those provided by the membrane manufacturer, i.e., between 10 and 15 nm. The pore area, for the same number of pores, ranges between 70 and 2539 nm², with an average value of 288 nm². The recovery rate calculated for these pores is 6.5 %. This value is in agreement with those provided by the membrane manufacture, i.e., recovery rate between 5 and 10 %.

The influence of the metallization step for this type of material was also studied. Indeed, in the case of cathodic sputtering, a coarse deposit is obtained, whose thermal effect is not significant. This shows that it is possible to characterize a cellulose acetate membrane (Fig. 2). However, in the case of the use of a metal coater using vacuum evaporation**,** the deposit is of course controlled, but a potential thermal effect has to be taken into account, resulting in a degradation of the polymer and therefore in the non visualization of the skin structure (Fig. 4). In conclusion of this part, optimum results were achieved using an accurate cathodic sputtering metal coater (controlled deposit).

3.2.2 PVDF membranes (membranes B)

A similar study was carried out on PVDF membranes with external skin. The influence of magnification and visualization repeatability on the equivalent pore diameter and on the pore area was studied. Fig. 5 shows the visualization of the PVDF membrane for two magnifications (× 100,000 and × 50,000). The values obtained from image processing for the two magnifications are given in Table 4. It is evident that the higher the magnification, the smaller the number of pores counted. The average values of the pore equivalent diameter remain the same, close to 12-15 nm. The measurement reproducibility for the same magnification is quite good, with an error of less than 3% on the average value. However, the magnification has an important effect on the recovery rate, which is doubled from 6.2% – 6.9% (× 50,000 magnification) to 13.5% (× 100,000 magnification). A similar observation can be made for membranes A with an increase in the recovery rate with increasing magnification. The determination for × 100,000 magnification being made on a poor

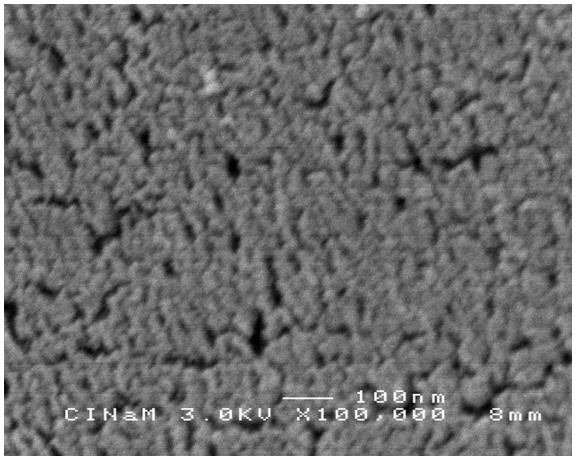

Fig. 5 External skin visualization of B membrane with a 5 nm gold layer, × 100,000 magnification (at the top) and × 50,000 magnification (2 images at the bottom)

Table 4 Influence of magnification on pore equivalent diameter and recovery rate for PVDF membrane

Magnification	Pore number	Mean pore equivalent diameter (nm)	Recovery rate (%)
× 50,000 (1)	1146	15.3	6.9
× 50,000 (2)	1034	14.9	6.2
× 100,000	752	12	13.5

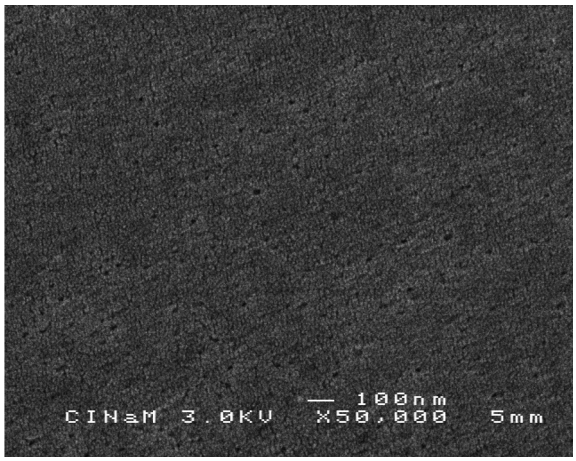

Fig. 6 External skin visualization of B membrane prepared by vapor deposition (× 50,000 magnification)

number of pores, it seems that the values obtained for the smallest magnification are the most reliable. As for the study of the equivalent pore diameter, a good reproducibility is obtained for the same magnification, with less than 10 % difference.

The effect of the metallization on these PVDF membranes was also studied. It seems that while a × 50,000 magnification makes it possible to analyze the images obtained with a cathodic sputtering metal coater (Fig. 5), a metallization by vacuum evaporation (Fig. 6) shows that if the pores are

visible, the degradation of the polymer can be observed and a more complex image processing is required, which is not necessarily relevant.

3.2.3 Conclusion and perspectives

The mapping of new membranes was performed on cellulose acetate, PVDF, PTFE and PES (not shown) hollow fiber membranes. However, a diameter of 5 to 8 nm, depending on the material (referring to pore size rather than to MWCO), seems to be the limit. Indeed, for cellulose acetate material or low cut-off, it appears that the polymer deteriorates if the magnification is excessively increased or if the shooting time is long. This is all the more important since SEM was operated at a low energy of 3 kV. SEM can reach up to 1 kV, which causes less damage but significantly decreases image sharpness: this is why a low energy of 3 kV was used. Besides, if a lower energy is employed, it is possible to limit or even cancel the thermal degradation and thus better determine the actual pore size. It is interesting to note that a cold cathode was used, which is recommended for insulating materials such as membranes. For the characterization of new membranes, the membrane geometry, the skin position in the hollow fiber geometry and the chemical nature of the

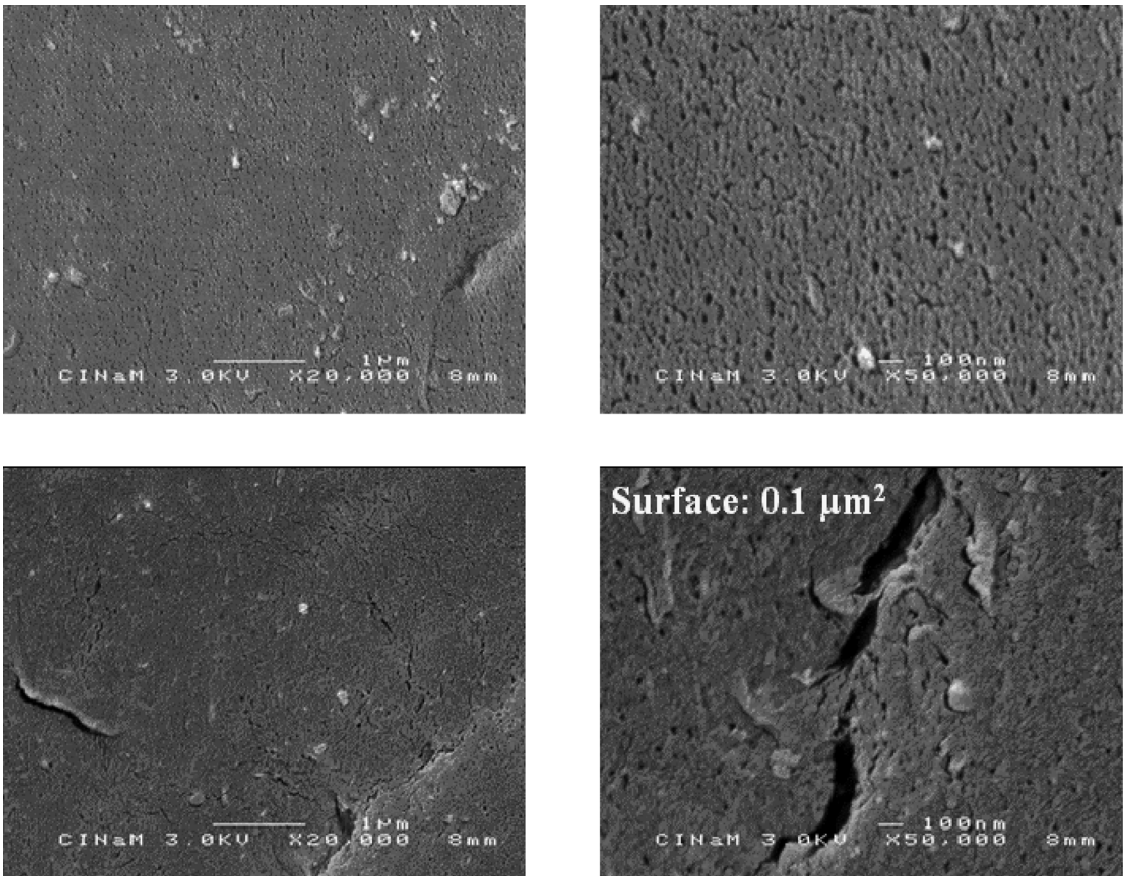

Fig. 7 Surface comparison of new (at the top) and used B membranes (at the bottom) for × 20 000 (left side) and × 50,000 (right side) magnification

material are not limiting parameters.

3.3 Ageing study on membranes B (PVDF)

The aim of this part is to study membrane ageing in the context of drinking water production from surface water. Different membranes from different sites (with and without pre-treatment) were studied. These membranes can be classified in 2 groups depending on the sample preparation. The AB (Aged B) membranes were membranes B extracted from the process after a backwash and the CB (Clean B) membranes were AB membranes washed by chemical cleaning. The reference membrane was the new PVDF membrane characterized in part 3.2.2.

3.3.1 9-month ageing at laboratory scale without pre-treatment

These membranes were used to produce drinking water without pre-treatment on laboratory scale. After 9 months ageing, the membranes showed a 65 % loss of permeability compared to a new membrane (from 300 to 105 $L.h^{-1}.m^{2}.bar^{-1}$). The first observations using HRSEM made it possible

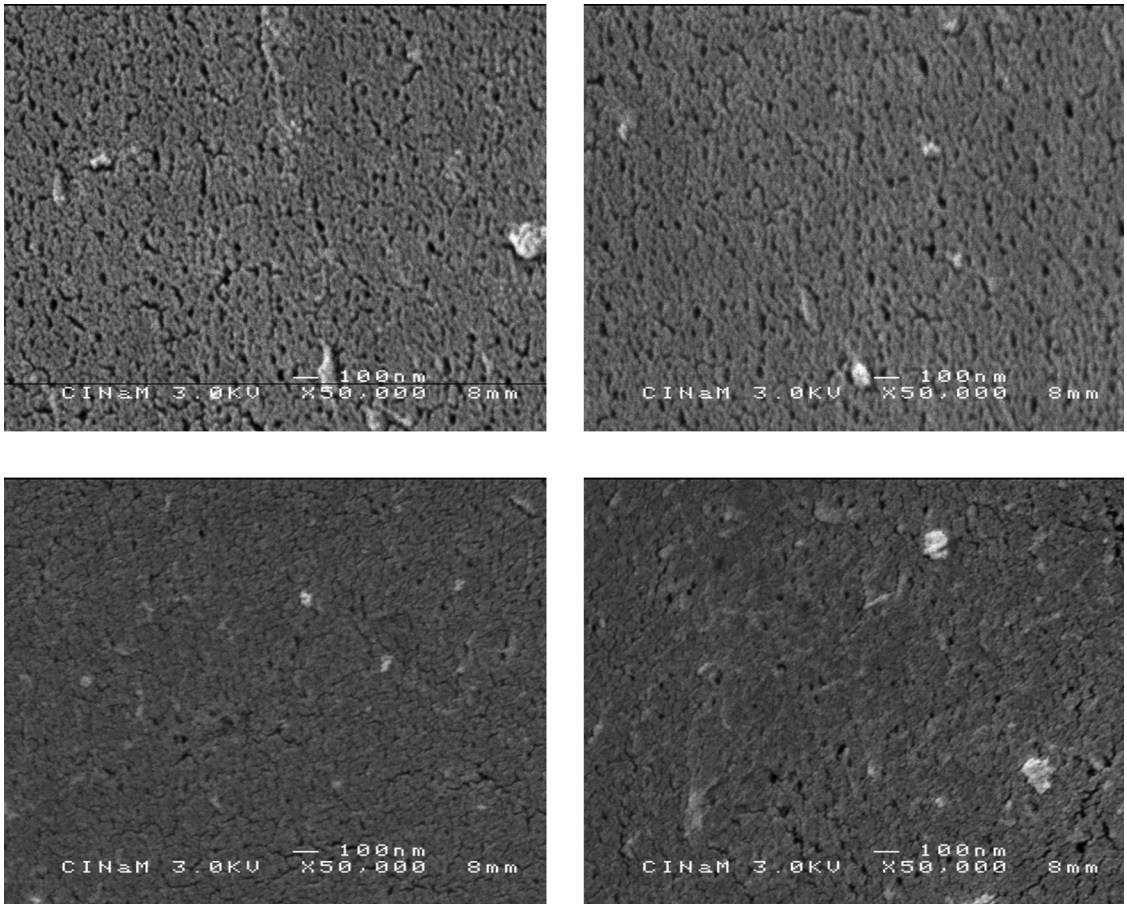

Fig. 8 Observation reproducibility of new (at the top) and used B membranes (at the bottom) for × 50,000 magnification

to conclude that there was a modification of the membrane surface (Fig. 7). Moreover, defects with a size reaching 0.1 μm² (Fig. 7) could be observed on the aged membranes. Modifications could be observed anywhere on the membrane surface for a given magnification (× 50,000; Fig. 8) or whatever the magnification (× 100,000; Fig. 9). The associated image processing reveals a decrease in all the parameters from new to aged membranes (Tables 5 and 6), whatever the magnification and the location on the membrane (noted 1 & 2). If there is a slight decrease in the mean equivalent pore diameter for × 50,000 magnification, a significant modification of the number of pores detected and of the recovery rate can be observed, with a 74% and 84% decrease, respectively. For × 100,000 magnification, a significant modification of the number of pores detected, of the mean equivalent pore diameter and of the recovery rate is observed, with a 55%, 25% and 61% decrease, respectively. In brief, it appears that a 65% drop in permeability may be related to a corresponding decrease in the number of pores coupled with a decrease in recovery rate. It appears that this protocol makes it possible to better understand the permeability drop highlighting fouling. It is also shown that the influence of the magnification is more significant for aged membranes and this is all the more true

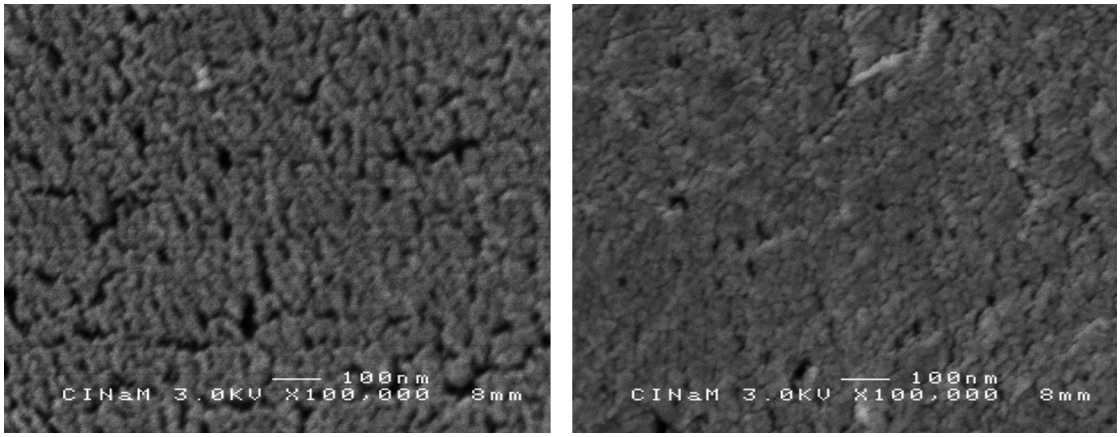

Fig. 9 Observation of new (right side) and used B membranes (left side) for × 100,000 magnification

Table 5 Comparison of pore equivalent diameter and recovery rate for new (B) and used (CB) membranes with × 50,000 magnification

Magnification	Pore number	Mean pore equivalent diameter (nm)	Recovery rate (%)
CB (1)	244	11.0	1.4
CB (2)	324	13.1	0.7
B (1)	1146	15.3	6.9
B (2)	1034	14.9	6.2

Table 6 Comparison of pore equivalent diameter and recovery rate for new (B) and used (CB) membranes with × 100,000 magnification

Magnification	Pore number	Mean pore equivalent diameter (nm)	Recovery rate (%)
CB	340	9.0	5.2
B	752	12.0	13.5

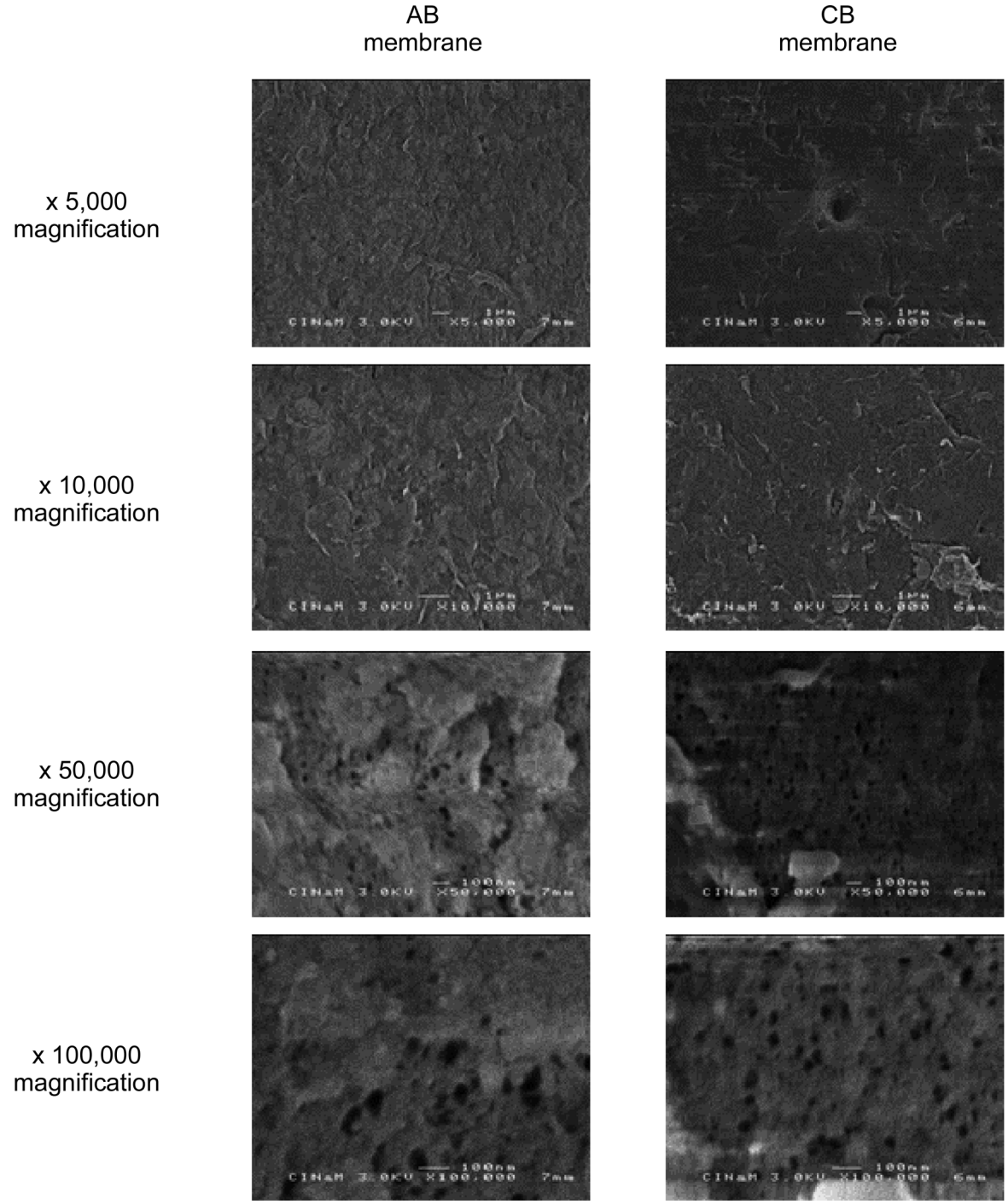

Fig. 10 Visualizations of B membrane ageed in pilot plant during 12 months before (AB membrane, left side) and after cleaning step (CB membrane, right side) at different magnifications (× 5,000, × 10,000, × 50,000 and × 100,000)

since membrane heterogeneity increases with ageing time. To define the optimal magnification, a maximum amount of process information is necessary. The purpose is not to provide the expected results but rather to look for considerable defects in the case of a loss of integrity as well as to identify a decrease in filtration properties (pore number and size) in the case of a loss of permeability.

3.3.2 12-month ageing at pilot scale with pre-treatment

The membranes used in this study were identical to those used previously although they differed in that they had been used for 12 months in an industrial drinking water plant. In the process, an aluminium coagulation-flocculation pre-treatment was carried out before membrane filtration. A 33 % permeability decrease was observed in this case: from 300 to 200 $L.h^{-1}.m^{2}.bar^{-1}$.

Experience feedback, the quality of the HRSEM images and the selection of an appropriate metallization step make it very clear that the surface of the membrane has been modified. Whatever the sample AB or CB (Fig. 10), the observed surface is very different from that of a new membrane (B). The "fluffy" surface appearance clearly shows that the observed skin is different from the skin of a new membrane: structural differences can be seen. The study of these visualizations (Table 7) shows that the equivalent pore diameter increases and the average value is close to 30 nm (29.7 nm). The analysis in terms of pore area shows occasional defects 1 μm in diameter and more systematically a recovery rate increased by a factor 2.

While the 9-month ageing without pre-treatment and the drop in permeability could be accounted for by the occurrence of a fouling phenomenon leading to a reduction in the average equivalent pore diameter, in the case of 12-month ageing with pre-treatment the average equivalent pore diameter is multiplied by 2. This is validated regardless of the magnification (× 50,000 × 100,000).

3.3.3 Conclusion on membranes B

Within the context of 9-month ageing of membranes without pre-treatment, judicious parameters explaining the loss of permeability were identified. However, the influence of the magnification is more important for an aged membrane and this is especially true when the membrane surface exhibits heterogeneities. Furthermore, within the framework of these HRSEM observations, it is essential to have a maximum of information about the membrane life.

Concerning aged membranes after 12-month ageing with pre-treatment, the "fluffy" surface appearance seems to indicate a modification of the membrane skin. The presence of important defects occasionally observed and clear scratches on the fiber surface also shows that the fiber external skin has undergone damage. The pore size is significantly increased from 12 nm (new membrane) to 26 nm (aged membrane). The increase is significant compared to the decrease observed on aged membranes after 9-month ageing without pre-treatment. However, this increase is still reasonable and can explain the decrease in log removal measured on site.

Table 7 Comparison of pore equivalent diameter at different magnification for membranes ageed in industrial pilot plant: aged membrane (AB) and clean membrane (CB)

Membranes	Magnification	Pore number	Mean pore equivalent diameter (nm)	Recovery rate (%)
AB	× 50,000	88	29.4	2.1
	× 100,000	39	32.3	4.2
CB	× 50,000	175	30.5	4.2
	× 100,000	111	26.7	7.7

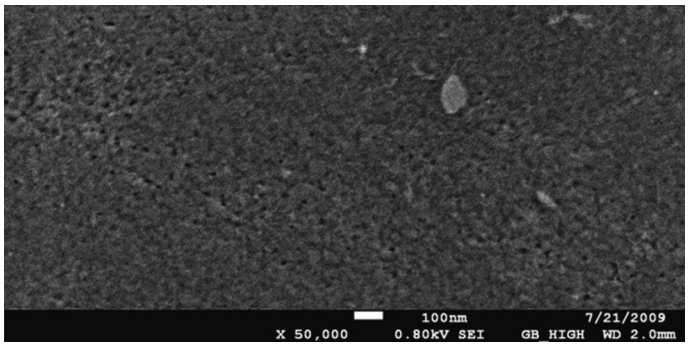

Fig. 11 External skin observation of PES hollow fiber membrane (MWCO = 80 kDa) with a 0.8 nm gold layer for × 50,000 magnification

4. Conclusion

In this study, it was possible to visualize the pores of organic membranes made of cellulose acetate, PVDF, PTFE or PES. These pores had a diameter greater than 5-8 nm depending on the material. Consequently, with the appropriate software and depending on the pore size, it was possible to obtain the evolution of the pore number as a function of the equivalent pore diameter and pore area. The minimum, maximum and average information for ultrafiltration membranes was calculated on a thousand pores. It was also possible to obtain the recovery rate. These observations were feasible on different materials, regardless of the membrane geometry and whatever the skin position in the hollow fiber and tubular geometry.

Three technical difficulties arose during this study. The first one was the sample preparation. Glycerine and other conditioning products had to be removed following a suitable washing protocol. It was found that static washing was not sufficient. The dynamic protocol proposed in the Material and Methods section was perfectly suitable for the membranes tested. The second difficulty arose from the thermal resistance of the polymer (cellulose acetate) - due to its nature or due to a low MWCO - requiring significant magnification with focalization of the electron beam on a small membrane area. To overcome this difficulty, exploration tests were performed using low energy HRSEM (0.8 kV), instead of the 3 kV used in this study. It was possible to carry out only a few tests (Fig. 11) and not on the entire study. Moreover, it is important to note that the energy of the HRSEM used in this study was already very low (3 kV). The third difficulty was the metallization step in the aim of visualizing the membrane pores. Thus, an optimal metal coater was used combining low thermal degradation (sputtering) with a controlled deposit. This is the type of metal coater advised for studies on organic membranes.

This study of membrane ageing showed that it is possible to relate the loss of permeability to a decrease in pore number and recovery rate. The presence or absence of pre-treatment on the same membrane can lead to very different observations.

References

Allen, T.D. and Goldberg M.W. (1993), "High-resolution SEM in cell biology", *Trends in Cell Biology*, **3**(6),

205-208.
Bottino, A., Capannelli, G., Grosso, A., Monticelli, O., Cavalleri, O., Rolandi, R. and Soria, R. (1994), "Surface characterization of ceramic membranes by atomic force microscopy", *J. Membrane Sci.*, **95**(3), 289-296.
Chahboun, A., Coratger, R., Ajustron, F., Beauvillain, J., Aimar, P. and Sanchez, V. (1992), "First investigations on the use of scanning tunnelling microscopy (STM) for the characterisation of porous membranes", *J. Membrane Sci.*, **67**(2-3), 295-300.
Chan, R. and Chen, V. (2004), "Characterization of protein fouling on membranes: opportunities and challenges", *J. Membrane Sci*., *Membrane Engineering Special Issue*, **242**(1-2), 169-188.
Chen, V., Li, H. and Fane, A.G. (2004), "Non-invasive observation of synthetic membrane processes - a review of methods", *J. Membrane Sci.*, **241**(1), 23-44.
Elimelech, M., Xiaohua, Z., Childress, A.E. and Seungkwan, H. (1997), "Role of membrane surface morphology in colloidal fouling of cellulose acetate and composite aromatic polyamide reverse osmosis membranes", *J. Membrane Sci.*, **127**(1), 101-109.
Hernández, A., Calvo, J.I., Prádanos, P. and Tejerina, F. (1998), "Pore size distributions of track-etched membranes; comparison of surface and bulk porosities", *Colloids and Surfaces A: Physicochemical and Engineering Aspects*, **138**(2-3), 391-401.
Hirose, M., Ito, H. and Kamiyama, Y. (1996), "Effect of skin layer surface structures on the flux behaviour of RO membranes", *J. Membrane Sci.*, **121**(2), 209-215.
Kim, K.J. and Fane, A.G. (1994), "Low voltage scanning electron microscopy in membrane research", *J. Membrane Sci.*, **88**(1), 103-114.
Hwang, K.J. and Lin, T.T. (2002), "Effect of morphology of polymeric membrane on the performance of cross-flow microfiltration", *J. Membrane Sci.*, **199**(1-2), 41-52.
Kim, K.J., Fane, A.G., Fell, C.J.D., Suzuki, T. and Dickson, M.R. (1990), "Quantitative microscopic study of surface characteristics of ultrafiltration membranes", *J. Membrane Sci.*, **54**(1-2), 89-102.
Kim, J.Y., Lee, H.K. and Kim, S.C. (1999), "Surface structure and phase separation mechanism of polysulfone membranes by atomic force microscopy", *J. Membrane Sci.*, **163**(2), 159-166.
Masselin, I., Durand-Bourlier, L., Laine, J.M., Sizaret, P.Y., Chasseray, X. and Lemordant, D. (2001), "Membrane characterization using microscopic image analysis", *J. Membrane Sci.*, **186**(1), 85-96.
Meieran, E.S. and Kamins, T.I. (1973), "High-resolution SEM observation of semiconductor device cross-sections", *Solid-State Electronics*, **16**(5), 545-548.
Pontie, M., Rapenne, S., Thekkedath, A., Duchesne, J., Jacquemet, V., Leparc, J. and Suty, H. (2005), "Tools for membrane autopsies and antifouling strategies in seawater feeds: a review", *Desalination*, **181**(1-3), 75-90.
Sheldon, J.M. (1991), "The fine-structure of ultrafiltration membranes. I. Clean membranes", *J. Membrane Sci.*, **62**(1), 75-86.
Tagawa, T., Mori, J., Aita, S. and Ogura, K. (1978), "Application of the high resolution SEM to the fine structure study of polyethylene", *Micron*, **9**(4), 215-221.
Warczok, J., Ferrando, M., Lopez, F. and Guell, C. (2004), "Concentration of apple and pear juices by nanofiltration at low pressures", *Journal of Food Engineering*, **63**(1), 63-70.
Wickramasinghe, S.R., Bower, S.E., Chen, Z., Mukherjee, A. and Husson, S.M. (2009). "Relating the pore size distribution of ultrafiltration membranes to dextran rejection", *J. Membrane Sci.*, **340**(1-2), 1-8.
Wu, Q. and Wu, B. (1995), "Study of membrane morphology by image analysis of electron micrographs", *J. Membrane Sci.*, **105**(1-2), 113-120.
Wyart, Y., Georges, G., Deumie, C., Amra, C. and Moulin, P. (2008), "Membrane characterization by microscopic methods: multiscale structure", *J. Membrane Sci.*, **315**(1-2), 82-92.
Xiuli, Y., Hongbin, C., Xiu, W. and Yongxin, Y. (1998), "Morphology and properties of hollow-fiber membrane made by PAN mixing with small amount of PVDF", *J. Membrane Sci.*, **146**(2), 179-184.
Zeman, L. and Denault, L. (1992), "Characterization of microfiltration membranes by image analysis of electron micrographs. : Part I. Method development", *J. Membrane Sci.*, **71**(3), 221-231.
Ziel, R., Haus, A. and Tulke, A. (2008), "Quantification of the pore size distribution (porosity profiles) in microfiltration membranes by SEM, TEM and computer image analysis", *J. Membrane Sci.*, **323**(2), 241-246.

ED